Heatline visualization of forced convection in porous media

Al. M. Morega and A. Bejan
Department of Mechanical Engineering and Materials Science, Duke University, Durham, NC, USA

The patterns of heatlines reported in this paper illustrate for the first time the true path of convective heat transfer through a saturated porous medium. Heatline patterns are reported for the following fundamental configurations: the boundary layer near an isothermal wall, the boundary layer near a wall with uniform heat flux, and the two-dimensional porous layer confined by two parallel plates. Emphasis is placed on the convection features that are being visualized for the first time by the heatline method, i.e., not by traditional methods such as the use of isotherms. It is shown that the heatlines of a flow in which the wall serves as heat sink are unlike the heatlines of the same flow with a wall that serves as heat source. The seepage flow with slip at the boundary is visualized by heatlines that leave a hot wall at an angle. The wall heat-flux distribution is visualized by the density of the heatlines that intersect the wall. The heatline pattern in fully developed flow of a pure fluid through a parallel-plate channel is also reported in order to emphasize that the pure-fluid pattern is not exactly the same as the pattern in the corresponding two-dimensional space filled with seepage flow through a porous medium.

Keywords: porous media; heatlines; forced convection

Introduction

The concepts of heatfunction and heatlines were introduced for the purpose of visualizing the true path of the flow of energy through a convective medium (Kimura and Bejan 1983; Bejan 1984). The heatfunction accounts simultaneously for the transfer of heat by conduction and convection at every point in the medium. The heatlines are a generalization of the flux lines used routinely in the field of conduction. The concept of heatfunction is a spatial generalization of the concept of Nusselt number, i.e., a way of indicating the magnitude of the heat transfer rate through any unit surface drawn through any point on the convective medium.

The first application of the heatline method was to the visualization of natural convection in an enclosure filled with fluid and heated from the side (Kimura and Bejan 1983). The method has been adopted in the heat transfer literature, and extended to several other convection configurations. Littlefield and Desai (1986) extended it to cylindrical coordinates and illustrated laminar natural convection in a vertical annular space. Trevisan and Bejan (1987) defined the equivalent concept of masslines in convection mass transfer, and used it to visualize natural convection driven by concentration gradients in a two-dimensional (2-D) rectangular enclosure. Aggarwal and Manhapra (1989a,b) employed heatlines in a study of unsteady natural convection in a cylindrical enclosure. Bello-Ochende (1987, 1988) visualized natural convection in tilted rectangular cavities and vertical square cavities heated from the side. Heatlines were also used to visualize natural convection in horizontal annuli (Ho et al. 1989; Ho and Lin 1989) and natural convection of cold water in a vertical annulus (Ho and Lin 1990).

Address reprint requests to Professor Bejan at the Department of Mechanical Engineering and Materials Science, Duke University, Box 90300, Durham, NC 27708-0300, USA.

Received 22 February 1993; accepted 23 August 1993

The common feature of these applications of the heatfunction method is that they all belong to the class of natural convection of pure fluids in enclosures. These flows are sufficiently complicated to require the use of numerical techniques, and this is why the heatfunction too had to be calculated numerically. On this background, the present paper contributes to the visualization of convective heat transfer in two ways:

(1) it extends the heatline method to the field of convection in porous media. This is the first-time application of the heatline method in a field that has seen tremendous growth during the past two decades (Kaviany 1992; Nield and Bejan 1992); and
(2) it shows that the heatfunction and the associated heatlines can be derived analytically in closed form. These expressions show analytically the superposition of local conduction and convection in the calculation of the heat transfer rate and its true path.

Boundary layer near a cold isothermal wall

In all the convection configurations discussed in this paper, it will be assumed that the porous medium is saturated with a single-phase fluid and that it can be modeled as homogeneous and isotropic. The solid and the fluid are locally in thermal equilibrium. One of the simplest convective flows of this kind is illustrated in Figure 1. The flow of far-field temperature T_∞ and volume-averaged velocity U_∞ is parallel to a plane isothermal surface of a different temperature, T_0.

The flow and temperature fields in the thermal boundary layer region are expressible in closed form (Bejan 1984, pp. 355–358):

$$u = U_\infty, \qquad v = 0 \tag{1}$$

$$\theta = \frac{T - T_0}{T_\infty - T_0} = \operatorname{erf}\left(\frac{\eta}{2}\right), \qquad \eta = y\left(\frac{U_\infty}{\alpha x}\right)^{1/2} \tag{2}$$

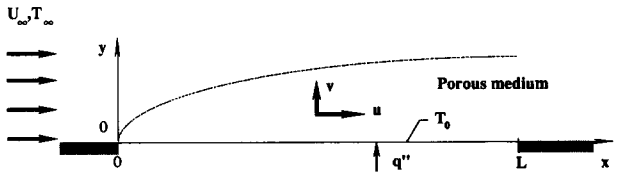

Figure 1 The thermal boundary layer near a heated or cooled section of the wall of a porous medium permeated by parallel flow

with the variables defined in the notation (see box). The parallel flow with slip at the wall, Equation 1, occurs in the Darcy and Darcy–Forchheimer regimes. The derivation of the heatfunction $H(x, y)$ associated with these flow and temperature fields begins with the observation that in the existing studies of convection in Cartesian coordinates (e.g., Bejan 1984), the longitudinal conduction term $k\,\partial^2T/\partial x^2$ was not negligible in the energy equation. The special feature of the boundary-layer region of Figure 1 is that $\alpha\,\partial^2T/\partial x^2$ is negligible in the energy equation,

$$u\frac{\partial T}{\partial x}+v\frac{\partial T}{\partial y}=\alpha\frac{\partial^2 T}{\partial y^2} \tag{3}$$

This feature demands a special definition for the heatfunction, so that H is valid inside the boundary-layer region

$$\frac{\partial H}{\partial y}=\rho c_P u(T-T_{ref}) \tag{4}$$

$$-\frac{\partial H}{\partial x}=\rho c_P v(T-T_{ref})-k\frac{\partial T}{\partial y} \tag{5}$$

It is easy to verify that the heatfunction $H(x, y)$ defined by Equations 4 and 5 satisfies the energy equation (Equation 3) identically, provided that the reference temperature T_{ref} is a constant. It was pointed out in Trevisan and Bejan (1987) that T_{ref} can have any value, and that the heatline pattern is not unique: there is one pattern for each T_{ref} value. It is also true that one heatline pattern can be more instructive to the eye than another. This is why in this paper T_{ref} will always be the lowest temperature that occurs in the convective medium that is being visualized. We begin with the assumption that the isothermal wall is colder than the seepage flow, $T_0 < T_\infty$, and set $T_{ref} = T_0$ for the remainder of this section. We will consider the reverse situation (hot wall, $T_0 > T_\infty$) in section 3.

If we substitute the flow and temperature solution (Equations 1 and 2) into the H definition (Equations 4 and 5), we obtain, in order,

$$\frac{\partial \tilde{H}}{\partial \tilde{y}}=\theta(\eta) \tag{6}$$

$$\frac{\partial \tilde{H}}{\partial \tilde{x}}=\frac{\partial \theta}{\partial \tilde{y}} \tag{7}$$

$$\tilde{x}=\frac{x}{L},\qquad \tilde{y}=y\left(\frac{U_\infty}{\alpha L}\right)^{1/2} \tag{8}$$

$$\tilde{H}=\frac{H}{k(T_\infty-T_0)\,\mathrm{Pe}_L^{1/2}} \tag{9}$$

and $\mathrm{Pe}_L = U_\infty L/\alpha$. Note that the quantity used as the denominator in the nondimensionalization of H is the scale of the total heat transfer rate through the surface of length L. We will return to this property of the dimensionless heatfunction $\tilde{H}$ at the end of this section. The result of integrating Equations 6 and 7 and using Equation 2 is

$$\tilde{H}(\tilde{x},\tilde{y})=\tilde{x}^{1/2}(\eta\theta+2\theta')$$
$$=\tilde{x}^{1/2}\left[\eta\,\mathrm{erf}\left(\frac{\eta}{2}\right)+\frac{2}{\pi^{1/2}}\exp\left(-\frac{\eta^2}{4}\right)\right] \tag{10}$$

The first line of Equation 10 shows the superposition of convection ($\eta\theta$) and transversal conduction ($2\theta'$) in the calculation of the local heat transfer rate (the heatfunction). The factor $g(\eta) = \eta\theta + 2\theta'$ is the similarity heatfunction profile. This function is as much a characteristic of the boundary layer as is the similarity temperature profile $\theta(\eta)$.

Figure 2 shows some of the $\tilde{H}$ = constant curves calculated based on Equation 10. This pattern of heatlines visualizes several features of convection near a cold wall. First, the energy that is eventually absorbed by the wall is brought into the boundary layer by fluid from upstream of the cold section of the wall. The boundary-layer region is delineated approximately by $\eta = 2$, which in Figure 2 is represented by the dotted line $\tilde{y} = 2\tilde{x}^{1/2}$.

Second, the heatlines that enter the wall are denser near $\tilde{x} = 0$. This is a way of visualizing the higher heat fluxes that exist near the tip, i.e., a wall heat flux that decays as $x^{-1/2}$ in the flow direction.

Third, the heatlines are perpendicular to the wall as they enter the wall. This is a consequence of the fact that the wall is colder than the distant medium, $T_{ref} = T_0$, which means that

Notation

c_P	Fluid specific heat at constant pressure
D	Wall-to-wall spacing
H	Heatfunction
$\tilde{H}$	Dimensionless heatfunction, Equation 9
$\hat{H}$	Dimensionless heatfunction, Equation 14
H_*	Dimensionless heatfunction, Equation 18
k	Thermal conductivity of porous medium saturated with fluid
L	Length of wall section with heat transfer
Nu	Nusselt number
Pe_L	Peclet number, $U_\infty L/\alpha$
Pe_D	Peclet number, UD/α
q''	Heat flux
T	Temperature
T_m	Mean temperature
T_{ref}	Reference temperature
T_0	Wall temperature
T_∞	Free-stream temperature
u	Longitudinal velocity
U	Mean velocity
U_∞	Free-stream velocity
v	Transversal velocity
x, y	Cartesian coordinates
$\tilde{x}, \tilde{y}$	Dimensionless coordinates, Equation 8
$\hat{x}, \hat{y}$	Dimensionless coordinates, Equation 22
X_T	Thermal entrance length

Greek symbols

α	Thermal diffusivity of saturated porous medium
η	Similarity variable, Equation 2
θ	Similarity temperature profile, Equation 2
ρ	Fluid density
τ	Similarity temperature profile, Equation 13

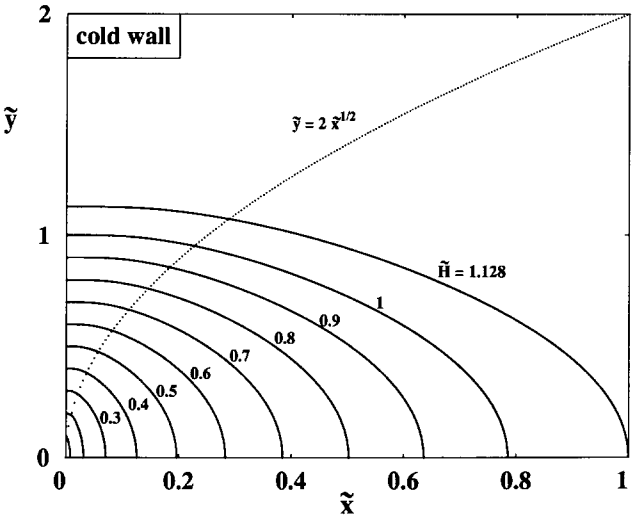

Figure 2 The boundary-layer heatlines near a cold isothermal wall

at the wall $\partial H/\partial y = 0$ (cf. Equation 4). It is important to note, however, that the perpendicularity of the heatlines at the wall is due to having chosen $T_{ref} = T_0$, i.e., to the convention that the reference temperature is the lowest temperature that occurs in the convective medium.

Fourth, the heatfunction increases along the wall because the wall absorbs the heat transfer released by the fluid. The dimensionless heatfunction increases from $\tilde{H} = 0$ at the tip to $\tilde{H} = 1.128$ at the trailing edge. According to Equation 9, the heatfunction at the trailing edge has the value $H(x = L, y = 0) = 1.128k(T_\infty - T_0)\,\mathrm{Pe}_L^{1/2}$. This trailing-edge H value matches exactly the total heat transfer rate through the wall of length L (e.g., Bejan, 1984, p. 358).

Boundary layer near a hot isothermal wall

Consider now the opposite arrangement in which the wall is warmer than the distant porous medium, $T_0 > T_\infty$. Since in this case the transfer of heat is from the wall to the flow, we expect a pattern of heatlines that differs markedly from that of Figure 2. The derivation of $H(x, y)$ begins with setting $T_{ref} = T_\infty$ in Equations 4 and 5 and follows the steps contained between Equations 6 and 10. Instead of $(T_\infty - T_0)$ in the denominator of the $\tilde{H}$ definition (Equation 9), we use the temperature difference $(T_0 - T_\infty)$, which is positive. For brevity, we list only the final result:

$$\tilde{H}(\tilde{x}, \tilde{y}) = \tilde{x}^{1/2}\left[\eta\,\mathrm{erfc}\left(\frac{\eta}{2}\right) - \frac{2}{\pi^{1/2}}\exp\left(-\frac{\eta^2}{4}\right)\right] \tag{11}$$

Figure 3 shows the pattern of heatlines that corresponds to the heatfunction of Equation 11. The heatlines come out of the wall at an angle because, unlike the situation in Figure 2, the gradient $\partial H/\partial y$ is not zero at the wall. Note that when the wall is warmer than the convective medium, the slip at $y = 0$ makes the right side of Equation 4 finite and constant, $\partial H/\partial y = \rho c_p U_\infty (T_0 - T_\infty)$. Even though $\partial H/\partial y$ is constant along the wall, the angle at which the heatlines emerge from the wall varies with x, because $(\partial H/\partial x)_{y=0}$ depends on x.

Above the wall, the heatlines are bent even more by the flow, as the effect of transversal conduction weakens. The denser heatlines near $\tilde{x} = 0$ indicate once again the higher fluxes that are known to be present near the leading edge of the heated section of the boundary. The wall heatfunction $\tilde{H}(\tilde{x}, 0)$ decreases as $\tilde{x}$ increases because the wall loses heat to the boundary layer. The trailing-edge heatfunction values $\tilde{H}(1, 0)$ corresponds to the total heat transfer rate released by the wall.

Overall, the heatlines occupy the same region as the boundary layer, and, since this region is physically slender, the heatlines are oriented almost in the same direction as the flow. This pattern is unlike the one seen near a cold wall (Figure 2), where the heatlines originate from upstream and cut across the boundary-layer region.

Boundary layer near a wall with uniform heat flux

We now turn our attention to the visualization of the thermal boundary layer when the wall section of length L releases the uniform heat flux q'' into the saturated porous medium of Figure 1. The solution for the temperature distribution in the thermal boundary layer with uniform flux was developed numerically and reported in Bejan (1984), pp. 358–359, 384–385). We use this opportunity to point out that the same solution can be expressed analytically in closed form,

$$T(x, y) = T_\infty + \frac{q''}{k}\left(\frac{\alpha x}{U_\infty}\right)^{1/2}\tau(\eta) \tag{12}$$

where the similarity temperature profile is

$$\tau(\eta) = \frac{2}{\pi^{1/2}}\exp\left(-\frac{\eta^2}{4}\right) - \eta\,\mathrm{erfc}\left(\frac{\eta}{2}\right) \tag{13}$$

The development of the boundary-layer heatfunction $H(x, y)$ follows the steps outlined in section 2. For brevity, we are omitting these steps while pointing out that the T_{ref} convention adopted under Equation 5 means that in Equations 4 and 5 we set $T_{ref} = T_\infty$, because the wall is warmer than the medium. The new dimensionless heatfunction $\hat{H}$ is defined as

$$\hat{H}(\tilde{x}, \tilde{y}) = \frac{H(x, y)}{q''L} \tag{14}$$

where $q''L$ is the total (known) heat transfer rate through the section of length L. In the end, the analytical expression that

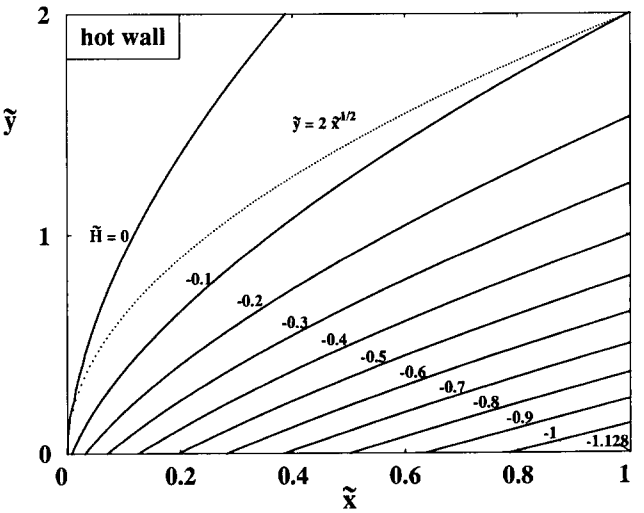

Figure 3 The boundary-layer heatlines near a hot isothermal wall

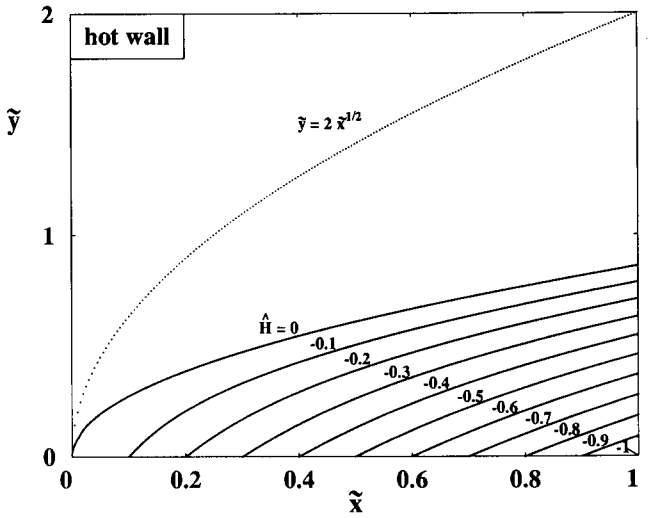

Figure 4 The boundary-layer heatlines near a hot wall with uniform flux

is obtained for the heatfunction is

$$\hat{H}(\tilde{x}, \tilde{y}) = \tilde{x}\left[\frac{\eta}{2}\tau(\eta) + \tau'(\eta)\right]$$

$$= \tilde{x}\left[\frac{\eta}{\pi^{1/2}}\exp\left(\frac{\eta}{2}\right) - \left(1 + \frac{\eta^2}{2}\right)\operatorname{erfc}\left(\frac{\eta}{2}\right)\right] \qquad (15)$$

The corresponding heatline pattern is shown in Figure 4, which can be compared directly with Figure 3 to see the effect of the uniform-flux boundary condition. The uniform flux is why in Figure 4 the heatlines that leave the wall are equidistant: note that the wall heatfunction decreases linearly while $\tilde{x}$ increases, $\hat{H}(\tilde{x}, 0) = -\tilde{x}$. The other features noted in the discussion of Figure 3 appear also in Figure 4. The trailing edge heatfunction value $\hat{H}(1, 0) = -1$ means that, from the tip to that location, the wall has released all the heat transfer of which it is capable.

Two-dimensional layer with hot isothermal walls

The preceding three sections dealt with the visualization of forced-convection boundary layers, which are an essential feature encountered in most external convection configurations. Consider now the phenomenon of internal convection, or convection in a confined porous medium. The simple form of forced convection in internal flow is presented in Figure 5. The parallel-plate channel of spacing D contains a saturated porous medium through which fluid seeps in uniform flow ($u = U$, $v = 0$) along x.

The heatlines of the entrance (or thermally developing) region will have features similar to those seen already in Figures 2 to 4. For this reason, we focus strictly on the fully developed region, and assume that its length L is at least one order of magnitude greater than the entrance length.

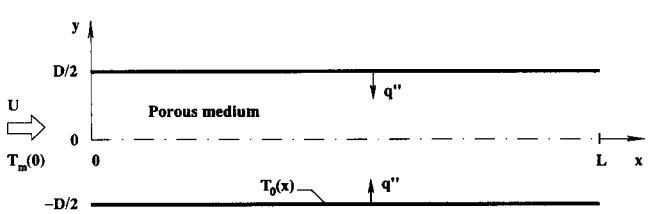

Figure 5 Forced convection in a 2-D porous layer confined by two parallel plates

In this section and the next, we assume that the walls are isothermal at T_0, while the fluid that enters through the $x = 0$ plane has the mean temperature $T_m(0)$. The temperature distribution in the saturated porous medium can be determined based on the classical approach, as for laminar flow through a pipe (e.g., Bejan 1984, pp. 89–91). The end result is

$$T(x, y) = T_0 - \frac{\pi}{2}\cos\left(\frac{\pi y}{D}\right)[T_0 - T_m(x)] \qquad (16)$$

with

$$\frac{T_0 - T_m(x)}{T_0 - T_m(0)} = \exp\left(-\frac{\pi^2 x}{D\,\mathrm{Pe}_D}\right), \qquad \mathrm{Pe}_D = \frac{UD}{\alpha} \qquad (17)$$

It is worth noting that the π^2 factor appearing in Equation 17 is the value of the Nusselt number based on the hydraulic diameter $2D$, namely, $\mathrm{Nu} = q''(x)2D/k[T_0 - T_m(x)] = \pi^2$.

The heatfunction $H(x, y)$ can be derived from Equations 4 and 5 by using the inlet temperature as the lowest temperature in the medium, $T_{ref} = T_m(0)$. For the heatfunction scale in the nondimensionalization of H, we used the total heat transfer rate released by the two walls in the limit where the channel is long enough so that $T_m(L) \cong T_0$. That scale is $\rho c_p UD[T_0 - T_m(0)]$; therefore, we set

$$H_* = \frac{H}{\rho c_p UD[T_0 - T_m(0)]} \qquad (18)$$

and after integrating Equations 4 and 5 in combination with Equations 16 and 17 and the flow solution ($u = U$, $v = 0$), we obtain

$$H_*(x, y) = \frac{y}{D} - \frac{1}{2}\sin\left(\frac{\pi y}{D}\right)\exp\left(-\frac{\pi^2 x}{D\,\mathrm{Pe}_D}\right) \qquad (19)$$

The distribution of heatlines in the 2-D porous layer with hot isothermal walls is shown in Figure 6. The heatlines in the immediate vicinity of the two walls are similar to what we saw in Figure 3 for the single boundary layer on a hot isothermal wall. The heatlines are inclined in the flow direction because of the flow slip condition. They become less dense as x increases because the heat flux decays exponentially in accordance with the exponential decay of the mean temperature difference (Equation 17).

Figure 6 provides a bird's-eye view of how only a certain section of the isothermal wall contributes in a real sense to the total heat transfer that is carried downstream by the fluid. That section is located upstream, where $x/(D\ \mathrm{Pe}_D)$ is less than about 0.5. The heatlines produced by this active section end up as a longitudinal bundle of parallel lines in the downstream section, i.e., in the region where the walls are inactive in a heat transfer sense. It is interesting that the heatlines in this longitudinal downstream bundle are equidistant, even though their points of origin on the walls are unevenly spaced.

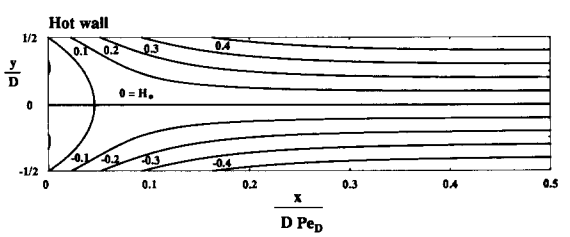

Figure 6 The heatlines in the fully developed region of the flow of Figure 5, when the walls are isothermal and hot

The fact that the cross formed by the two $H_* = 0$ lines is visible in Figure 6 is an indication that 1) the leading section of the channel was blown up, and 2) that $H_* = 0$ was assigned to the corner points ($x = 0$, $y = \pm D/2$). The latter condition is the result of having chosen the heatfunction length scale listed above (Equation 18), which is the correct length scale when the channel is "long enough" such that $T_m(L) \cong T_0$, i.e., when the abscissa group $x/D\ \mathrm{Pe}_D$ is much greater than 1. Note that if Figure 6 is replotted to show the entire (i.e., the proper) range of relevant abscissa values, all the way to $x/D\ \mathrm{Pe}_D \gg 1$, the crossing of the $H_* = 0$ lines becomes invisible (see the top drawing of Figure 8).

Two-dimensional layer with cold isothermal walls

The analytical expression for the heatfunction in a layer with cold isothermal walls can be derived using the same approach as in the preceding section. One difference is that the reference temperature is now the wall temperature, $T_{ref} = T_0$. The dimensionless heatfunction H_* is defined as in Equation 18, except that the positive difference $[T_m(0) - T_0]$ replaces the temperature difference shown in the denominator in Equation 18. We omit the algebra and give only the final expression:

$$H_*(x, y) = \frac{1}{2} \sin\left(\frac{\pi y}{D}\right) \exp\left(-\frac{\pi^2 x}{D\ \mathrm{Pe}_D}\right) \tag{20}$$

Figure 7 shows the constant-H_* lines recommended by Equation 20. They show how the energy is brought into the porous medium by the hot fluid, and how it is later deposited on the cold walls. Only the upstream wall section of order $x/(D\ \mathrm{Pe}_D) \sim 0.2$ is active as a heat sink. The heatlines are now perpendicular to the wall at the point where they cross the wall. This feature was encountered also in the boundary layer on a cold isothermal wall (see Figure 2).

The main conclusion to be drawn from Figure 7 is that the pattern of heatlines changes dramatically as the role of the walls switches from that of heat source (Figure 6) to heat sink (Figure 7). This dramatic change was made visible also by Figures 2 and 3.

Comparison with the heatlines of fully developed flow in a parallel-plate channel with pure fluid

Finally, it is worth mentioning that the heatline patterns drawn in Figures 6 and 7 for the 2-D porous layer are identical to the heatlines of a parallel-plate channel with pure fluid in "slug" flow ($u = U_\infty$, $v = 0$). For the pure fluid, the k and α values that are involved in Equations 16 to 20 are properties of the fluid.

The immediate question, then, is what happens to the pure-fluid heatlines if, instead of the assumed slug flow, the

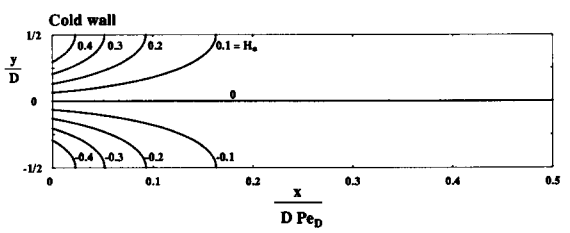

Figure 7 The heatlines in the fully developed region of the flow of Figure 5, when the walls are isothermal and cold

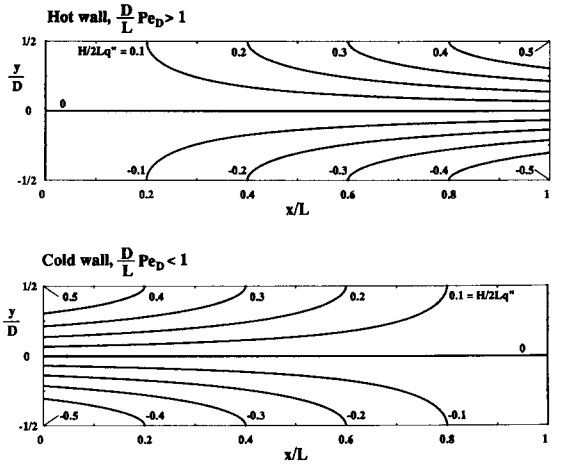

Figure 8 The heatlines in the fully developed flow of a pure fluid through a parallel-plate channel with uniform heat flux

parallel-plate channel contains the real fully developed flow. To answer this question analytically, we assumed that the heat flux q'' is distributed uniformly over the wall length L (the T_0 = constant case would require numerical work). For conciseness we give only the final results. The heatfunction for the channel with hot walls, $T_0(x) > T_m(x)$, is

$$\frac{H}{2Lq''} = \hat{x}\left(\frac{3}{4}\hat{y} - \frac{1}{4}\hat{y}^3\right) + \frac{1}{128}\frac{D}{L}\mathrm{Pe}_D\left(-\frac{117}{35}\hat{y} + \frac{249}{35}\hat{y}^3 - \frac{21}{5}\hat{y}^5 + \frac{3}{7}\hat{y}^7\right) \tag{21}$$

where

$$\hat{x} = \frac{x}{L}, \qquad \hat{y} = \frac{y}{D/2} \tag{22}$$

The corresponding result for the channel with cold walls, $T_0(x) < T_m(x)$, is

$$\frac{H}{2Lq''} = (1 - \hat{x})\left(\frac{3}{4}\hat{y} - \frac{1}{4}\hat{y}^3\right) + \frac{1}{128}\frac{D}{L}\mathrm{Pe}_D\left(-15\hat{y} + 11\hat{y}^3 - \frac{21}{5}\hat{y}^5 + \frac{3}{7}\hat{y}^7\right) \tag{23}$$

The heatline patterns described by Equations 21 and 23 are presented in Figure 8. One important observation is that the group $(D/L)\ \mathrm{Pe}_D$, which appears in the above expressions, has a negligible effect on the heatlines because it is less than 10 in an order-of-magnitude sense,

$$\frac{D}{L}\mathrm{Pe}_D < 10 \tag{24}$$

such that Equation 23 is replaced approximately by

$$\frac{H}{2Lq''} \cong (1 - \hat{x})\left(\frac{3}{4}\hat{y} - \frac{1}{4}\hat{y}^3\right) \tag{25}$$

Inequality 24 stems from the observation that the length of the fully developed section, L, is greater than the thermal entrance length X_T, where $X_T \sim 10^{-1} D\ \mathrm{Pe}_D$ (Bejan 1984, p. 96).

The uniform heat-flux thermal boundary condition is visualized by the equidistant heatlines that cross the parallel plates. The general outlook of the heatline pattern changes from

the case of the hot wall (Figure 8, top) to that of the cold wall (Figure 8, bottom), in the same way as in going from Figure 6 to Figure 7 in the two 2-D porous layer.

One important feature that distinguishes Figure 8 from Figures 6 and 7 is that in pure-fluid fully developed flow the heatlines are always normal to the wall, regardless of whether the wall is hot or cold. This feature visualizes the no-slip condition ($u = 0$ at $y = \pm D/2$), which distinguishes the flow of the pure fluid from the seepage flow of Figures 1–7. Note that in pure fluids the no-slip condition leads to $\partial H/\partial y = 0$ on the walls (cf. Equation 4), regardless of the value chosen for T_{ref}.

Conclusions

In this paper we displayed the heatline patterns of the most basic forced-convection flows in porous media. These patterns illustrate for the first time the true path of convective heat transfer in the configurations of Figures 1 and 5 and in the more complex configurations that involve forced-convection boundary layers and channel flows. The fundamental nature of the simple configurations of Figures 1 and 5 permitted us to develop the associated heatfunctions in closed form and to demonstrate analytically the superposition of convection and conduction at every point in the convective medium.

Since the objective of this study was to contribute to the visualization of convection in porous media, it is appropriate to review some of the convection features that are visualized by heatlines and not by a traditional method such as the use of isotherms:

(1) the heat transfer path through a medium in which the wall serves as heat source is unlike the path through the same medium (and flow) in which the wall serves as heat sink (compare, for example, the boundary layer in Figures 2 and 3 or the 2-D layer in Figures 6 and 7);
(2) the flow with slip past a hot boundary is visualized by heatlines that are inclined at an angle as they leave the boundary (see Figures 3 and 6);
(3) the distribution of wall heat flux is visualized by the density of the heatlines that cross that wall. Figures 2, 3, 6, and 7 illustrate the uneven distribution of heat flux along isothermal walls, while Figures 4 and 8 show the equidistant heatlines that emerge from a wall with uniform heat flux; and
(4) the heatline pattern in a parallel-plate channel with pure fluid in fully developed flow is not identical to the pattern in the same parallel-plate space filled with a saturated porous medium with fully developed seepage flow.

Acknowledgment

This work was made possible by a grant from the North Carolina Supercomputing Center.

References

Aggarwal, S. K. and Manhapra, A. 1989a. Use of heatlines for unsteady buoyancy-driven flow in a cylindrical enclosure. *J. Heat Transfer*, **111**, 576–578

Aggarwal, S. K. and Manhapra, A. 1989b. Transient natural convection in a cylindrical enclosure nonuniformity heated at the top wall. *Numer. Heat Transfer A*, **15**, 341–356

Bejan, A. 1984. *Convection Heat Transfer*. Wiley, New York, 21–23, 450–452

Bello-Ochende, F. L. 1987. Analysis of heat transfer by free convection in tilted rectangular cavities using the energy analogue of the stream function. *Int. J. Mech. Eng. Education*, **15**, 91–98

Bello-Ochende, F. L. 1988. A heat function formulation for thermal convection in a square cavity. *Int. Comm. Heat Mass Transfer*, **15**, 193–202

Ho, C. J. and Lin, Y. H. 1989. Thermal convection heat transfer of air/water layers enclosed in horizontal annuli with mixed boundary conditions. *Wärme-und Stoffübertragung*, **24**, 211–224

Ho, C. J. and Lin, Y. H. 1990. Natural convection of cold water in a vertical annulus with constant heat flux on the inner wall. *J. Heat Transfer*, **112**, 117–123

Ho, C. J., Lin, Y. H., and Chen, T. C. 1989. A numerical study of natural convection in concentric and eccentric horizontal cylindrical annuli with mixed boundary conditions. *Int. J. Heat Fluid Flow*, **10**, 40–47

Kaviany, M. 1992. *Principles of Heat Transfer in Porous Media*. Springer-Verlag, New York

Kimura, S. and Bejan, A. 1983. The "heatline" visualization of convective heat transfer. *J. Heat Transfer*, **105**, 916–919

Littlefield, D. and Desai, P. 1986. Buoyant laminar convection in a vertical cylindrical annulus. *J. Heat Transfer*, **108**, 814–821

Nield, D. A. and Bejan, A. 1992. *Convection in Porous Media*. Springer-Verlag, New York

Trevisan, O. V. and Bejan, A. 1987. Combined heat and mass transfer by natural convection in a vertical enclosure. *J. Heat Transfer*, **109**, 104–109